TELECOM
ParisTech

# NL-InSAR : Non-Local Interferogram Estimation

## NL-InSAR : estimation non-locale d'interférogrammes

Charles-Alban Deledalle
Loïc Denis
Florence Tupin

**2009D021**

novembre 2009

Département Traitement du Signal et des Images
Groupe TII : Traitement et Interprétation des Images

# NL-InSAR: Estimation Non-Locale d'Interférogrammes

Charles-Alban Deledalle, Loïc Denis et Florence Tupin

**Résumé**

Les données interférométriques radar à synthèse d'ouverture (InSAR) fournissent des images de réflectivité, de différence de phase et de cohérence, qui sont essentielles pour l'interprétation de l'image et les traitements de bas niveaux tels que la segmentation et la reconstruction 3D. Ces images sont obtenues en pratique à partir du produit hermitien estimé sur des fenêtres locales. Ces fenêtres produisent un biais et une perte de résolution au niveau des contours et des textures due à leur hétérogénéité spatiale. Ce rapport propose une approche non-locale pour l'estimation conjointe des images de réflectivité, de différence de phase et de cohérence à partir d'un couple interférométrique d'images radar complexes mono-vues (SLC) préalablement recalées. Les techniques non-locales sont connues pour réduire efficacement le bruit sans dégrader les structures de l'image en procédant à une moyenne pondérée des pixels similaires. Deux pixels sont considérés comme similaires si les patchs qui les recouvrent sont ressemblants. La similarité entre patchs est communément définie par la distance euclidienne entre les vecteurs de niveaux de gris. Elle n'est pas applicable aux images radar interférométrique perturbées par un bruit de speckle. Dans ce rapport, un critère de similarité entre patchs, basé sur des considérations statistiques, est dérivé pour les images SLC. Une estimation au sens du maximum de vraisemblance pondérée est réalisée avec des poids obtenus à partir des données InSAR. Ces poids sont définis sur l'intensité et la différence de phase, et sont itérativement raffinés par la similarité entre patchs bruités et par la similarité des patchs de l'estimation précédente. L'efficacité de cette nouvelle technique de construction des interférogrammes est illustrée qualitativement et quantitativement sur des données synthétiques et réelles.

**Mots-clés**

Estimation, moyennes non-locales, interférométrie radar à synthèse d'ouverture (InSAR)

C. Deledalle et F. Tupin sont à l'Institut Telecom, Telecom ParisTech, CNRS LTCI, Paris, France, e-mail: charles-alban.deledalle@telecom-paristech.fr et florence.tupin@telecom-paristech.fr.

L. Denis est à l'École Supérieure de Chimie Physique Électronique de Lyon et au Laboratoire Hubert Curien, CNRS UMR 5516, St-Étienne, France, e-mail: loic.denis@cpe.fr.

# NL-InSAR: Non-Local Interferogram Estimation

Charles-Alban Deledalle, Loïc Denis et Florence Tupin

## Abstract

Interferometric synthetic aperture radar (InSAR) data provides reflectivity, phase difference and coherence images, which are paramount to scene interpretation or low-level processing tasks such as segmentation and 3D reconstruction. These images are estimated in practice from hermitian product on local windows. These windows lead to biases and resolution losses due to local heterogeneity caused by edges and texture. This paper proposes a non-local approach for joint estimation of the reflectivity, phase difference and coherence images from an interferometric pair of co-registered single-look complex (SLC) SAR images. Non-local techniques are known to efficiently reduce noise while preserving structures by performing a weighted averaging of similar pixels. Two pixels are considered similar if the surrounding image patches are "resembling". Patch-similarity is usually defined as the Euclidean distance between the vectors of graylevels. In this paper a statistically grounded patch-similarity criterion suitable to SLC images is derived. A weighted maximum likelihood estimation of the SAR interferogram is then computed with weights derived in a data-driven way. Weights are defined from intensity and phase difference, and are iteratively refined based both on the similarity between noisy patches and on the similarity of patches from the previous estimate. The efficiency of this new interferogram construction technique is illustrated both qualitatively and quantitatively on synthetic and true data.

## Index Terms

Estimation, non-local means, interferometric synthetic aperture radar (InSAR)

C. Deledalle et F. Tupin sont à l'Institut Telecom, Telecom ParisTech, CNRS LTCI, Paris, France, e-mail: charles-alban.deledalle@telecom-paristech.fr et florence.tupin@telecom-paristech.fr.

L. Denis est à l'École Supérieure de Chimie Physique Électronique de Lyon et au Laboratoire Hubert Curien, CNRS UMR 5516, St-Étienne, France, e-mail: loic.denis@cpe.fr.

## I. INTRODUCTION

Interferometric synthetic aperture radar (InSAR) aims to recover information about heights or displacements in a scene. Two SAR complex images are sensed by two parallel-passes separated by a spatial baseline. The amplitude components provide information on the reflectivity, and, after co-registration of the two images, the phase difference is directly related to the path delay between the two waves. This phase difference can be used to recover the height or the movement [1]. The amplitudes and the phase differences are damaged by speckle noise. Due to temporal and spatial variations between the two acquisitions, the speckle components between the two acquisitions present a small decorrelation which affects the phase difference. The coherence between the two acquisitions appears then as a crucial indicator of the reliability of the phase difference. This paper focuses on the joint estimation of the three InSAR parameters: the reflectivity of the scene, the phase difference and the coherence. Note that the orbital component of the interferometric phase is assumed to have been previously removed from the phase images to insure the phase stationarity in homogeneous areas.

An interferometric pair of co-registered single-look complex (SLC) SAR images can be well-modeled on each pixel with a joint parametric distribution grounded on three physical parameters: the reflectivities, the actual phase difference and the coherence. Let $z$ and $z'$ be two complex values of two corresponding pixels in the two SLC images. According to Goodman's model [2], $z$ and $z'$ follow a zero-mean complex circular Gaussian distribution:

$$p(z, z'|\Sigma) = \frac{1}{\pi^2 det(\Sigma)} \exp\left[ -(z^* z'^*) \, \Sigma^{-1} \begin{pmatrix} z \\ z' \end{pmatrix} \right] \tag{1}$$

with $\Sigma$ a $2 \times 2$ covariance matrix, which can be decomposed as follows:

$$\begin{aligned} \Sigma &= \mathbb{E}\left\{ \begin{pmatrix} z \\ z' \end{pmatrix} (z^* z'^*) \right\} \\ &= \begin{pmatrix} R & \sqrt{RR'}De^{j\beta} \\ \sqrt{RR'}De^{-j\beta} & R' \end{pmatrix} \end{aligned} \tag{2}$$

where $R$ and $R'$ are the underlying reflectivities, $\beta$ the actual phase difference, $D$ the coherence between the two acquisitions and $\mathbb{E}$ denotes the mathematical expectation.

Numerous estimators have been proposed to estimate the covariance matrix $\Sigma$. The majority have been specially designed to estimate only one of the three parameters:

- Amplitude denoising is usually achieved by using spatially adaptive filtering based on local statistics in order to cope with the signal-dependent multiplicative speckle noise [3]–[7]. We refer the reader

to the survey of R. Touzi [8] for a deeper analysis of such methods. The most recent approaches use parametric distributions based wavelet soft-thresholding, with spatially adaptive filtering in the wavelet domain [9], [10], or with logarithmically transformed amplitude [11]–[13]. Non-local estimation of the reflectivity has been also proposed in [14].

- Phase difference restoration is usually expressed as a problem of phase denoising and phase unwrapping. This paper focuses only on the first problem namely the estimation of the noise-free wrapped phase difference. Recent techniques achieve this goal by finding the best local polynomial approximation in an adaptive window [15]–[17].

- The coherence is an indicator of the reliability of the phase quality but is also widely used to detect temporal changes in remote sensing applications. The main problem in the coherence estimation is the introduction of a bias toward highest values due to the low number of averaged samples. Different methods have been proposed to improve the quality of the estimation in terms of bias and variance [18]–[20].

Other estimators take advantage of the Goodman's model to provide a joint estimation of the three parameters. The majority of them are based on local statistics, and therefore affect the spatial resolution while few estimators achieve this goal without significant loss of resolution:

- The usual parameter estimation approach is the direct application of the spatial coherence principle. It considers noisy samples in a window centered on a given pixel as all following the distribution of that pixel. This leads to the boxcar filter which locally estimates the complex covariance matrix $\Sigma$ over a sliding window. Known as complex multi-looking, this operation is largely used in practice to provide an estimate of the reflectivity, the actual phase difference and the coherence. The fundamental limitation of this technique comes from the loss of resolution on the estimated images, since the same smoothing effect is equally applied to homogeneous regions, and to edges or textured zones. Moreover, as mentioned above, the coherence estimate is biased toward highest values due to the low number of samples in the local window.

- In [21], [22], Lee *et al.* proposed to use adaptive filtering for polarimetric and interferometric SAR denoising. Instead of estimating the parameters over a rectangular sliding window, a directional window is locally selected among eight edge-aligned windows, according to the local gradient of the amplitude images. A complex covariance matrix is estimated over the obtained window which is used in the linear minimum mean square error estimator to obtain the denoised covariance matrix $\Sigma$. This preserves edge structures, since values of pixels on each side of the edge are never combined

together, avoiding then smoothing effects. Unfortunately, this methods tends to leave a high variance in homogeneous area and create some undesired artifacts.

- Intensity-driven adaptive-neighborhood (IDAN) technique has been proposed in [23] for polarimetric and interferometric SAR parameter estimation. Following the idea of filtering over directional windows, IDAN performs a complex multi-looking operation on an adaptive neighborhood. This adaptive neighborhood is constructed with a region growing algorithm where the most similar adjacent pixels are selected iteratively according to their intensity values. The adaptive neighborhood aims to select as many pixels as possible, all following the same statistical population as the given pixel. This decreases the bias (i.e, resolution loss) in the estimation since noisy values coming from other populations are rejected. However, due to its connectivity constraint, IDAN leaves a high variance in regions where there are only few adjacent similar pixels.

One may think that similar pixels are present in a local neighborhood such as rectangular windows, directional windows or spatially connected components. Instead, similar pixels can be considered as far apart. Our idea, based on the non-local means filter [24], is that SAR images present lots of redundant patterns which can be used to select a large set of pixels to combine for the estimation of each given pixel. A pixel is assumed to come from the same statistical population as the given pixel if the patches that surround the two pixels are similar. This patch-based estimator can be considered as *non-local* since pixel values somewhat far apart can be averaged together, depending on the surrounding patch-similarity. The non-local interferometric SAR (NL-InSAR) estimator is based on the patch-based estimator introduced in [14] for image denoising. Instead of combining pixels from a binary set, a membership value is computed according to a patch-based similarity criterion. This membership value is then used in a weighted maximum likelihood estimator to produce the desired parameters. Unlike directional windows based filtering and IDAN which use only the intensity to select the suitable samples, NL-InSAR uses a probabilistic criterion based on both the intensities and the phase differences that surround two given patches (it is assumed that the orbital component has been previously removed from the phase images). Moreover, the estimation is refined iteratively by including the similarity between pre-estimated patches of the parameters. This iterative process noticeably improves the estimation performances.

## II. Non-Local Estimation

### A. Weighted Maximum Likelihood Estimation

This section presents the method proposed for NL-InSAR to estimate the three parameters $R$, $\beta$ and $D$. It seems reasonable to consider equal the (true) reflectivities of each pair of corresponding pixels,

i.e $R = R'$ in (2). This hypothesis is naturally verified in regions with good coherence. By reducing the number of degrees of freedom (from 4 to 3 unknowns), the estimation variance is improved. Denoising techniques must trade-off variance reduction and resolution preservation. As the sample size is restricted by resolution preservation considerations, it is desirable to reduce the variance with such a hypothesis. Let $A = |z|$ and $A' = |z'|$ be the amplitudes and $\phi = \arg(zz'^*)$ the noisy phase difference. From (1) and (2), with the constraint $R = R'$, the InSAR observations are related to the InSAR parameters $R, D$ and $\beta$ by [25]:

$$p(A, A', \phi | R, D, \beta) = \frac{4AA'}{\pi^2 R^2 (1 - D^2)} \times$$
$$\exp\left(-\frac{A^2 + A'^2 - 2DAA'\cos(\phi - \beta)}{R(1 - D^2)}\right). \tag{3}$$

NL-InSAR is based on the weighted maximum likelihood estimator (WMLE) where the weights are defined in a patch-based approach. Formally, the WMLE defines at each site $s$ the estimate $\hat{\Theta}_s = (\hat{R}_s, \hat{\beta}_s, \hat{D}_s)$ as:

$$\hat{\Theta}_s = \arg\max_{\Theta} \sum_t w(s, t) \log p(\mathcal{O}_t | \Theta) \tag{4}$$

where $\mathcal{O}_t = (A_t, A'_t, \phi_t)$ is the observation at site $t$ and $w(s, t) > 0$ is a data-driven weight. WMLE is known to reduce the mean squared error by reducing the variance of the estimate at the cost of a bias introduced by samples that follow a distribution with parameters $\Theta_t$ different to $\Theta_s$ [26]. The WMLE framework has already been applied successfully to image denoising in [27] and [14]. For InSAR data, the maximum likelihood estimator of the covariance matrix $\Sigma$ is well-known to be the sample estimate of the covariance matrix. The parameters $R$, $R'$, $\beta$ and $D$ are then given by term identification which leads to compute the sample estimate of the complex cross-correlation. Seymour and Cumming in [28] derived the maximum likelihood estimator of (3) which differs from the classical sample estimate since it assumes that $R = R'$. When this assumption holds, it is shown in [28] that their estimator is more efficient than the classical sample estimate. For instance, an estimate of the coherence can be obtained without complex multi-looking. From their work, we extend their formulation to the case of WMLE, which is given, for $\Theta_s = (R_s, \beta_s, D_s)$ and $\mathcal{O}_t = (A_t, A'_t, \phi_t)$, by:

$$\hat{R}_s = \frac{a}{2N},$$
$$\hat{D}_s = \frac{2}{a}\left(x\cos\hat{\beta}_s + y\sin\hat{\beta}_s\right),$$
$$\hat{\beta}_s = -\arg(x + jy) \tag{5}$$
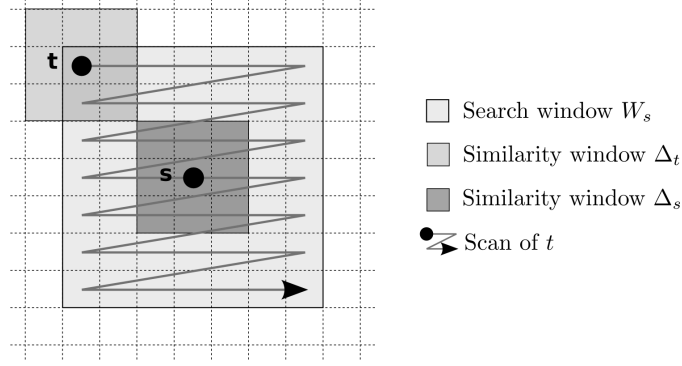$$\text{with} \quad a = \sum_t w(s, t)\left(A_t^2 + A'^2_t\right),$$

Figure 1. WMLE combines for each site $s$ the information of pixels $t$ according to the similarity between two patches $\Delta_s$ and $\Delta_t$ centered respectively around the sites $s$ and $t$.

$$
\begin{aligned}
x &= \sum_t w(s,t) Re\left[z_t z_t'^*\right], \\
y &= \sum_t w(s,t) Im\left[z_t z_t'^*\right], \\
N &= \sum_t w(s,t).
\end{aligned}
\tag{6}
$$

In [14], we take inspiration of the non-local means algorithm to define the weights $w(s,t)$. The two observations $\mathcal{O}_s$ and $\mathcal{O}_t$ are assumed to come from the same statistical population, i.e $\Theta_s = \Theta_t$, if the patches $\Delta_s$ and $\Delta_t$ that surround the two pixels $s$ and $t$ are similar. Figure 1 illustrates the procedure. At each site $s$, the pixels $t$ are inspected sequentially to produce a weight by comparing the two noisy patches $\Delta_s$ and $\Delta_t$. Once all weights $w(s,t)$ are computed, the WMLE is obtained according to (4). Note that for complexity reasons, the pixels $t$ are restricted to a large window $W_s$ centered around the site $s$. In the non-local means the similarity between the two patches $\Delta_s$ and $\Delta_t$ is given by an Euclidean distance of the intensity values. On InSAR data, such a distance cannot be used directly since it does not consider the statistical nature of the multi-dimensional observations. In [14], we showed that the Euclidean distance can be substituted by a similarity criterion grounded on statistical considerations for non-additive or non-Gaussian noises. The same approach can be applied here for InSAR data.

*B. Similarity between noisy patches*

The similarity between the two patches $\Delta_s$ and $\Delta_t$ can be defined according to the likelihood that the two patches $\Delta_s$ and $\Delta_t$ have identical parameters given the noisy observations $\mathcal{O}$: $\prod_k Pr(\mathcal{O}_{s,k}, \mathcal{O}_{t,k} | \Theta_{s,k} = \Theta_{t,k})$ where $_{s,k}$ and $_{t,k}$ denotes the $k$-th pixel in each patch $\Delta_s$ and $\Delta_t$ [14]. Since this likelihood function

is unknown, we define the weights with respect to a function $f$ which fits as well as possible the likelihood function:

$$w(s,t) \triangleq \prod_k f(\mathcal{O}_{s,k}, \mathcal{O}_{t,k} | \Theta_{s,k} = \Theta_{t,k})^{1/h} \tag{7}$$

where $h$ is a filtering parameter. For reason of readability, the pixels $_{s,k}$ and $_{t,k}$ will be denoted respectively by $_1$ and $_2$ in the following. Under the assumption that the two observations $\mathcal{O}_1$ and $\mathcal{O}_2$ come from the same statistical population, i.e $\Theta_1 = \Theta_2$, then the probability density function (pdf) of the similarity likelihood is obtained by considering all possible values of the unknown parameter $\Theta$ [29]. This leads to the following relation:

$$p(\mathcal{O}_1, \mathcal{O}_2 | \Theta_1 = \Theta_2) \propto \int p(\mathcal{O}_1 | \Theta_1 = \Theta) p(\mathcal{O}_2 | \Theta_2 = \Theta) \mathrm{d}\Theta. \tag{8}$$

Note that (8) holds by assuming the prior densities $p(\Theta_1 = \Theta)$ and $p(\Theta_2 = \Theta)$ are uniform improper densities. Unfortunately, the pdf is not necessarily scale-invariant which is not satisfying to model the weights in the WMLE. However, its definition depends on the chosen observation space of $\mathcal{O}$. The choice of $\mathcal{O}$ affects the pdf by a multiplicative factor namely the Lagrangian. Then, the search of a suitable observation space can lead to obtain a scale-invariant similarity likelihood. Given the pdf function of the original observation $\mathcal{O}$ and $\Phi$ a mapping function from the original observation space to the suitable observation space, the function $f$ can be defined as:

$$f(\mathcal{O}_1, \mathcal{O}_2 | \Theta_1 = \Theta_2) = \left| \frac{d\Phi}{d\mathcal{O}_1}(\mathcal{O}_1) \right|^{-1} \left| \frac{d\Phi}{d\mathcal{O}_2}(\mathcal{O}_2) \right|^{-1} p(\mathcal{O}_1, \mathcal{O}_2 | \Theta_1 = \Theta_2). \tag{9}$$

In case of InSAR data, a simple dimensional analysis shows that $\Phi : (A, A', \phi) \mapsto (\sqrt{A}, \sqrt{A'}, \phi)$ is a good choice to have a scale-invariant similarity likelihood. According to the suitable $\Phi$, equation (9) and appendix A, the similarity likelihood, for $\mathcal{O}_k = (A_k, A'_k, \phi_k)$, $k = 1..2$, is given by:

$$f(\mathcal{O}_1, \mathcal{O}_2 | \Theta_1 = \Theta_2) = \sqrt{\frac{\mathcal{C}}{\mathcal{B}}}^3 \left( \frac{\mathcal{A} + \mathcal{B}}{\mathcal{A}} \sqrt{\frac{\mathcal{B}}{\mathcal{A} - \mathcal{B}}} - \arcsin \sqrt{\frac{\mathcal{B}}{\mathcal{A}}} \right) \tag{10}$$

$$\text{with} \quad \mathcal{A} = (A_1^2 + A_1'^2 + A_2^2 + A_2'^2)^2,$$
$$\mathcal{B} = 4(A_1^2 A_1'^2 + A_2^2 A_2'^2 + 2A_1 A_1' A_2 A_2' \cos(\phi_1 - \phi_2)),$$
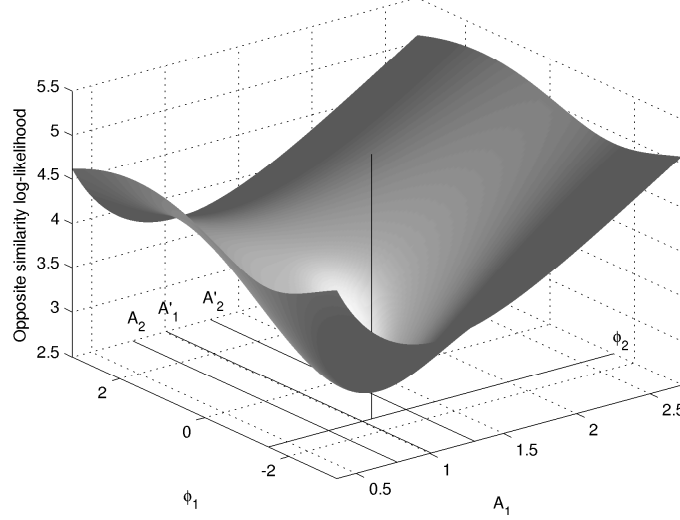$$\mathcal{C} = A_1 A_1' A_2 A_2'.$$

Figure 2. Similarity log-likelihood with respect to $A_1$ and $\phi_1$ for the given values $A_1'$, $A_2$, $A_2'$ and $\phi_2$.

Figure 2 represents the similarity likelihood defined in (10) with respect to the values of $A_1$ and $\phi_1$ for given values of $A_1'$, $A_2$, $A_2'$ and $\phi_2$. To emphasize the variations of the similarity likelihood, the negative logarithm of the similarity likelihood $-\log f(\mathcal{O}_1, \mathcal{O}_2|\Theta_1 = \Theta_2)$ is plotted. The criterion is minimum when observed data are identical: $A_1 = A_2$, $A_1' = A_2'$ and $\phi_1 = \phi_2$. Moreover, this criterion manages well with the phase wrapping, without creating discontinuities when $\phi_1$ moves from $-\pi$ to $\pi$. For a given value of $A_1$, the criterion is minimum when $\phi_1$ and $\phi_2$ are in-phase and maximum when they are out of phase. An interesting property of the similarity likelihood is that for a given pair of observed phases $\phi_1$ and $\phi_2$, the criterion is more discriminant when the observed amplitudes come closer, and is less discriminant when the amplitudes move away.

### C. Similarity between pre-estimated patches

In [14], it has been proposed to refine the weights iteratively by using at iteration $i$ the previously estimated parameters $\hat{\Theta}^{i-1}$. Instead of approaching the similarity likelihood, we try to approach the *a posteriori* probability defined by the Bayes relation:

$$Pr(\Theta_1 = \Theta_2|\mathcal{O}) \propto \underbrace{Pr(\mathcal{O}_1, \mathcal{O}_2|\Theta_1 = \Theta_2)}_{\text{likelihood term}} \times \underbrace{Pr(\Theta_1 = \Theta_2)}_{\textit{prior term}} \tag{11}$$

The idea is to use the pre-estimated image $\hat{\Theta}^{i-1}$ to measure the validity of the hypothesis $\Theta_1 = \Theta_2$. The equality $\Theta_1 = \Theta_2$ is assumed to be more likely to hold as the data distributions with parameters $\hat{\Theta}_1^{i-1}$ and $\hat{\Theta}_2^{i-1}$ get closer. Polzehl and Spokoiny showed that the Kullback-Leibler divergence between these
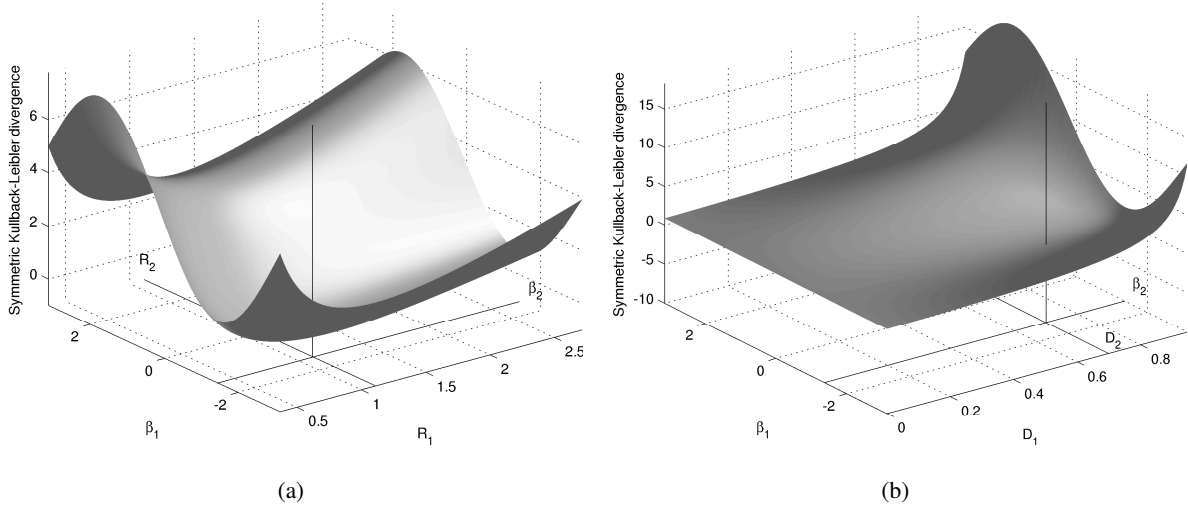
Figure 3. Symmetric Kullback-Leibler divergence with respect to (a) $\hat{R}_1$ and $\hat{\beta}_1$ for the given values of $\hat{R}_2$, $\hat{\beta}_2$ with $\hat{D}_1 = \hat{D}_2 = 0.7$, and (b) $\hat{D}_1$ and $\hat{\beta}_1$ for the given values of $\hat{\beta}_2$, $\hat{D}_2$ with $\hat{R}_1 = \hat{R}_2$.

two data distributions provides a statistic test of the hypothesis $\Theta_1 = \Theta_2$ [27]. The *prior* term is defined by a symmetrical version of the Kullback-Leibler divergence over an exponential decay function:

$$Pr(\Theta_1 = \Theta_2) \propto \exp\left[-\frac{1}{T}SD_{KL}(\hat{\Theta}_1^{i-1}, \hat{\Theta}_2^{i-1})\right]$$

$$\text{where } SD_{KL}(\hat{\Theta}_1^{i-1}, \hat{\Theta}_2^{i-1}) =$$

$$\int \left(p(\mathcal{O}|\hat{\Theta}_1^{i-1}) - p(\mathcal{O}|\hat{\Theta}_2^{i-1})\right) \log \frac{p(\mathcal{O}|\hat{\Theta}_1^{i-1})}{p(\mathcal{O}|\hat{\Theta}_2^{i-1})} \, d\mathcal{O} \tag{12}$$

and $T > 0$ is a positive real value. The parameters $T$ and $h$ act as dual parameters to balance the trade-off between the noise reduction and the fidelity of the estimate [27]. According to appendix B, the symmetrical Kullback-Leibler divergence in (12), for $\hat{\Theta}_k = \left(\hat{R}_k, \hat{\beta}_k, \hat{D}_k\right)$, $k = 1..2$, is given by:

$$SD_{KL}(\hat{\Theta}_1, \hat{\Theta}_2) = \frac{4}{\pi}\left[\frac{\hat{R}_1}{\hat{R}_2}\left(\frac{1 - \hat{D}_1\hat{D}_2\cos(\hat{\beta}_1 - \hat{\beta}_2)}{1 - \hat{D}_2^2}\right) + \right.$$

$$\left. \frac{\hat{R}_2}{\hat{R}_1}\left(\frac{1 - \hat{D}_1\hat{D}_2\cos(\hat{\beta}_1 - \hat{\beta}_2)}{1 - \hat{D}_1^2}\right) - 2\right].$$

$$\tag{13}$$

Figure 3 represents the symmetric Kullback-Leibler divergence defined in (13). In 3.a, the variations are given with respect to the values of $\hat{R}_1$ and $\hat{\beta}_1$, for given values of $\hat{R}_2$ and $\hat{\beta}_2$ with $\hat{D}_1 = \hat{D}_2 = 0.7$. In 3.b, the variations are given with respect to the values of $\hat{\beta}_1$ and $\hat{D}_1$, for given values of $\hat{\beta}_2$ and $\hat{D}_2$ with $\hat{R}_1 = \hat{R}_2$. The criterion decreases when all parameters at pixel $_1$ get closer to the parameters at pixel $_2$ and becomes null when the parameters are equal. Moreover, this criterion manages well with the

phase wrapping, without creating discontinuities when $\hat{\beta}_1$ moves from $-\pi$ to $\pi$. For a given value of $\hat{R}_1$, the criterion is minimum when $\hat{\beta}_1$ and $\hat{\beta}_2$ are in-phase and maximum when they are out of phase. An interesting property of this criterion is that the similarity of the phase parameters gains in importance when the coherence comes higher, since it means that the phase parameters are more reliable.

### D. Enforcing a minimum amount of smoothing

It is desirable to enforce a minimum amount of smoothing (i.e., variance reduction) in the denoising technique. In an image, some patches are (almost) unique (i.e., not found elsewhere inside the search window). The direct application of the algorithm would produce highly noisy estimates for the central value of these patches since the weighted maximum likelihood estimation would be computed over too few samples. In [14] this was not an issue for amplitude denoising. When considering iterative joint amplitude-phase-coherence estimation, the high variance of the estimator for "rare" patches leads to a decrease of the similarity between pre-estimated patches with the iterations. At the algorithm end, the resulting denoised images contains regions of high residual variance.

To guarantee a minimum amount of smoothing, and therefore limit the variance of the estimation, we propose to estimate the equivalent number of looks of the denoised pixels. Due to our non-local (data driven) approach, the equivalent number of looks varies from one pixel to another. It depends on the number of similar patches found in the search window, and can be approximated, for each pixel $s$, by:

$$\hat{L}_s = \frac{\left(\sum_t w(s,t)\right)^2}{\sum_t w(s,t)^2} \tag{14}$$

according to the variance reduction of a weighted average for the reflectivity and [17] for the phase difference. To enforce a minimum amount of smoothing, we suggest to redefine the weights $w(s,t)$ in the cases where the equivalent number of looks $\hat{L}_s$ falls below a given threshold $L_{min}$. An option is to redistribute equally the weights of the $L_{min}$ most similar patches whenever $\hat{L}_s < L_{min}$. "Rare' patches often contain a bright scatterer. To prevent from biaising the estimation, we propose to restrict the selection of the $L_{min}$ patches to those whose central value is not too bright compared to that of the reference patch, following the ideas of [30]–[32]. The correction of the weights can be performed as follows:

- Compute $\hat{L}_s$ for each pixel $s$,
- If $\hat{L}_s < L_{min}$, redistribute the $L_{min}$ highest weights:
  - Create a vector $\mathbf{w}$ containing all the weights $w(s,t)$ such that $A_t < 2A_s$,
  - Sort the vector $\mathbf{w}$ in descending order,

---

**Algorithm** Non Local InSAR (NL-InSAR)

---

**Input:** $\mathcal{O} = (A, A', \phi)$ and $\hat{\Theta}^{i-1} = \left( \hat{R}^{i-1}, \hat{\beta}^{i-1}, \hat{D}^{i-1} \right)$

**Output:** $\hat{\Theta}^i = \left( \hat{R}^i, \hat{\beta}^i, \hat{D}^i \right)$

**for all** pixels $s$ of the image **do**

    Initialize the accumulators $a, x, y$ and $N$ to zero

    **for all** pixels $t$ in $W_s$ **do**

        $\log w(s, t) \leftarrow 0$

        **for all** pixels $s, k$ and $t, k$ in $\Delta_s$ and $\Delta_t$ **do**

            Compute $f(\mathcal{O}_{s,k}, \mathcal{O}_{t,k} \mid \Theta_{s,k} = \Theta_{t,k})$

                            $\triangleright$ use Eq. 10

            Compute $SD_{KL}(\hat{\Theta}_{s,k}^{i-1}, \hat{\Theta}_{t,k}^{i-1})$     $\triangleright$ use Eq. 13

            $\log w(s, t) \leftarrow \log w(s, t)$

                $+ \frac{1}{h} \log f(\mathcal{O}_{s,k}, \mathcal{O}_{t,k} \mid \Theta_{s,k} = \Theta_{t,k})$

                $- \frac{1}{T} SD_{KL}(\hat{\Theta}_{s,k}^{i-1}, \hat{\Theta}_{t,k}^{i-1})$

        **end for**

        Increment the accumulators $a, x, y$ and $N$

                              $\triangleright$ use Eq. 6

    **end for**

    Insure a minimum noise reduction     $\triangleright$ see Sec. II-D

    Compute $\hat{\beta}_s^i, \hat{D}_s^i$ and then $\hat{R}_s^i$     $\triangleright$ use Eq. 5

**end for**

**return** $\left( \hat{R}^i, \hat{\beta}^i, \hat{D}^i \right)$

---

Figure 4. Pseudo-code of the non local InSAR algorithm. The procedure has to be repeated iteratively. At iteration $i$ the pre-estimated parameters $\hat{R}^{i-1}$, $\hat{\beta}^{i-1}$, $\hat{D}^{i-1}$ are used to refine the estimates. In practice, the first pre-estimates can be chosen as constant parameter images, and at least ten iterations have to be performed to reach the best estimate.

   &ndash; Redistribute equally the weights of the $L_{min}$ most similar pixels:

$$\mathbf{w}_k \leftarrow \frac{1}{L_{min}} \sum_{l=1}^{L_{min}} \mathbf{w}_l \quad \forall k \in 0..L_{min} \tag{15}$$

## III. Algorithm

This section describes the whole procedure used in NL-InSAR. At each site $s$, the pixels $t$ present in the search window $W_s$ are inspected sequentially to produce a weight by comparing two surrounding

patches $\Delta_s$ and $\Delta_t$. For each corresponding pixels $s,k$ and $t,k$ in $\Delta_s$ and $\Delta_t$, the similarity is computed by comparing noisy observations $\mathcal{O}_{s,k}$ and $\mathcal{O}_{t,k}$ (10) and the pre-estimated parameters $\hat{\Theta}_{s,k}^{i-1}$ and $\hat{\Theta}_{t,k}^{i-1}$ (13). These similarities are aggregated to produce the weights $w(s,t)$. In practice, the logarithm of the weights is computed to limit numerical errors. The weight $w(s,t)$ is then used to increment the accumulators $a, x, y$ and $N$ (6). Once all weights are obtained for each site $t$, the minimum noise reduction procedure is performed (Section II-D) before computing the parameters $\hat{\Theta}_s^i$ (5). The procedure is performed iteratively. Indeed, at the end of the iteration $i-1$, the estimated parameters provide the pre-estimated parameters $\hat{\Theta}^{i-1}$ used at iteration $i$. The procedure is repeated until there is no more change between two consecutive estimates. In practice, the first pre-estimates can be chosen as constant parameter images, and at least ten iterations have to be performed to reach the best estimate.

The pseudo-code of NL-InSAR is given in Figure 4. The algorithm complexity is $O(|\Omega||W||\Delta|)$ where $|\Omega|$, $|W|$ and $|\Delta|$ are respectively the image size, the search window size and the similarity patch-size. Several optimizations of the non-local means have been proposed in [33]–[35]. We have extended the solution proposed by Darbon $et\ al.$ in [36] for the NL-InSAR algorithm with a time complexity given by $O(4|\Omega||W|)$. Finally, the computational time of our method is of about 160 seconds per iteration for an image of size $|\Omega| = 512 \times 512$ and windows of size $|W| = 21 \times 21$ and $|\Delta| = 7 \times 7$ using an Intel Pentium D 3.20GHz.

## IV. EXPERIMENTS AND RESULTS

### A. Results on Synthetic Data

This section presents qualitative and numerical results obtained on simulated InSAR data. Given the true images of reflectivity $R$, phase difference $\beta$ and coherence $D$, two single-look complex (SLC) images $z_1$ and $z_2$ are generated according to the model presented in section I. The simulation procedure, similar to that for simulating a polarimetric InSAR image [21], is as follow:

- Compute a matrix $L$ such that $\Sigma = LL^*$. For example, the lower triangle matrix $L$ in the Cholesky decomposition is a good candidate:

$$L = \sqrt{R} \begin{pmatrix} 1 & 0 \\ De^{-j\beta} & \sqrt{1-D^2} \end{pmatrix}, \tag{16}$$

- Generate two independent complex random variables $x_1$, $x_2$ according to (1) with an identity covariance matrix,
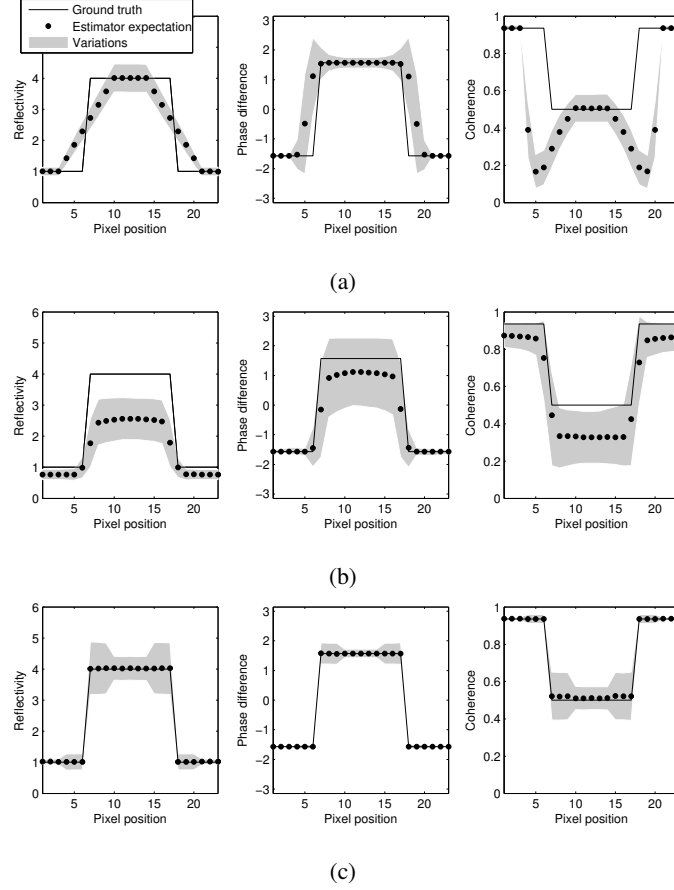
Figure 5.   Statistical answer on a rectangular function for (a) the boxcar estimator, (b) the IDAN estimator and (c) the NL-InSAR estimator.

• Finally, the correlated complex random variables $z_1$, $z_2$ are given by:

$$\left( \begin{array}{c} z_1 \\ z_2 \end{array} \right) = L \left( \begin{array}{c} x_1 \\ x_2 \end{array} \right). \tag{17}$$

Once the two SLC SAR images are generated, the three InSAR parameters are estimated and compared to the known actual parameters. Our NL-InSAR estimator is applied with a search window of size $|W| = 21 \times 21$ and a similarity window of size $|\Delta| = 7 \times 7$. The parameters $h$ and $T$ are set as described in [14]. A minimum noise reduction of level $L_{min} = 10$ is maintained. We use 10 iterations of the iterative NL-InSAR filter to reach a satisfying estimation. Comparisons have been performed with the classical boxcar filter on a $7 \times 7$ sliding window and the IDAN filter with an adaptive neighborhood of maximum size 50 [23].
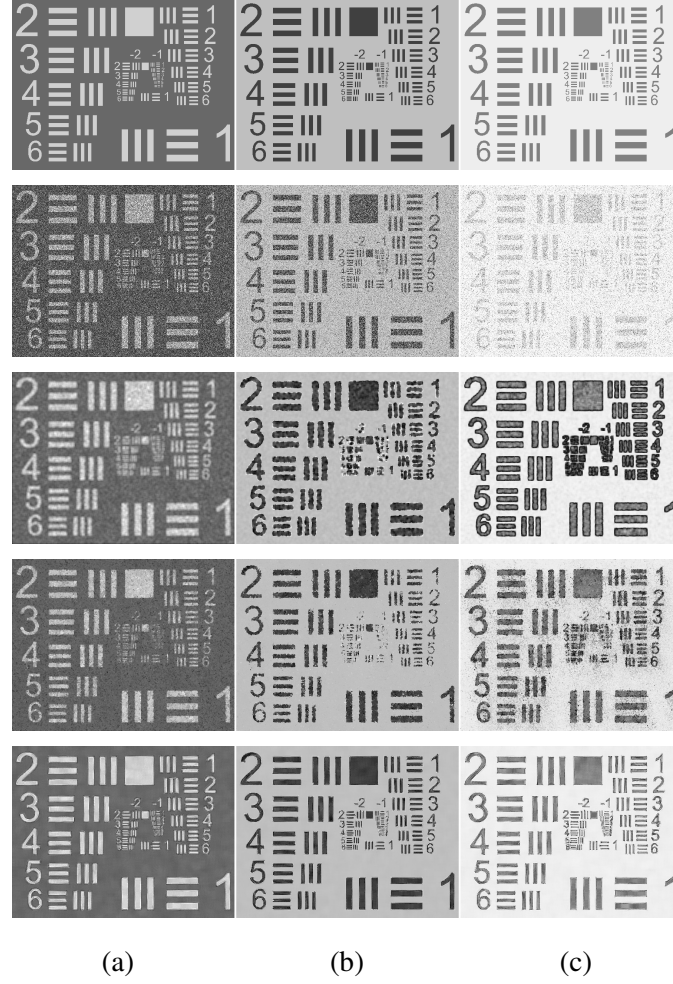
Figure 6. (a) Reflectivity, (b) phase difference and (c) coherence of a resolution test pattern obtained from top to bottom by the gound truth, the SLC images (maximum likelihood estimator of [28]), the boxcar estimator, the IDAN estimator [37] and the NL-InSAR estimator.

Figure 5 shows the statistical answer of the three estimators on a cut through a line of width 10. The statistics have been measured on denoised images over 10 000 noisy generated images. The ground truth, the mean and an interval of variation (about 70% of the estimates) is represented on the graphics for the three estimated components. It can be noticed that the boxcar filter is unbiased with a low variance in homogeneous area but it presents a strong spatial bias around the edges of the rectangular function. This spatial bias produces large underestimations of the coherence around edges wich is denoted in [21] as the dark ring effect. IDAN introduces a bias in homogeneous area due to the region growing method which tends to lower reflectivity and coherence values [23]. Moreover, the bias increases on the line since the adaptive neighborhood selects samples out of the line. As a result the variance is bigger than the

Table I

SNR VALUES OF ESTIMATED INSAR IMAGES USING DIFFERENT ESTIMATORS

|  | Reflectivity | Phase difference | Coherence |
|---|---|---|---|
| SLC Image [28] | -2.75 | 3.36 | -1.19 |
| WIN-SAR [13] | 5.22 | - | - |
| PEARLS [16] | - | 5.27 | - |
| Boxcar filter | 6.47 | 5.90 | -4.01 |
| IDAN [37] | 5.00 | 7.88 | 0.33 |
| NL-InSAR | **9.02** | **13.04** | **6.92** |

boxcar filter even if there are as many values to estimate the cross-correlation. NL-InSAR provides the best bias-variance trade-off. Indeed, comparatively to the boxcar filter and IDAN, NL-InSAR is neither biased in homogeneous area nor around edges. Moreover, its variance is equivalent to the one of the boxcar filter in homogeneous area. NL-InSAR has a bigger variance around edges than in homogeneous area since these regions present less redundant patterns.

Figure 6 presents the obtained estimated images for two generated single-look complex images representing a resolution test pattern. The images obtained with the NL-InSAR estimator seem to be well smoothed with a better edge and shape preservation. The images obtained by the boxcar and the IDAN estimators are more noisy than the images obtained by the NL-InSAR filter (the remaining variance is larger). Moreover, the boxcar estimator blurs the edges resulting to a loss of resolution and large underestimations of the coherence around edges. The IDAN filter preserves the shapes but the noise variance remains large essentially in the coherence image, and small details are lost essentially in the phase difference image. Finally, our NL-InSAR estimator seems to work efficiently by preserving small structures with a satisfying noise reduction.

To quantify the estimation qualities, Table I presents numerical results for the resolution test pattern presents on Figure 6. The performance criterion used is the Signal to Noise Ratio (SNR)

$$SNR(\hat{u}, u) \quad = \quad 10 \log_{10} \frac{Var[u]}{\frac{1}{|\Omega|} \sum_{s \in \Omega} (u_s - \hat{u}_s)^2}. \tag{18}$$

where $u$ is one of the actual component and $\hat{u}$ its estimate. Note that for the phase difference, we measure the SNR of the complex phase image $e^{j\hat{\beta}}$ to deal with phase wrapping as proposed in [16]. The results in term of SNR are compared again with the boxcar filter, IDAN and also with WIN-SAR [13] (a wavelet based amplitude filter) and PEARLS [16] (an adaptive local phase filter). NL-InSAR outperforms all the
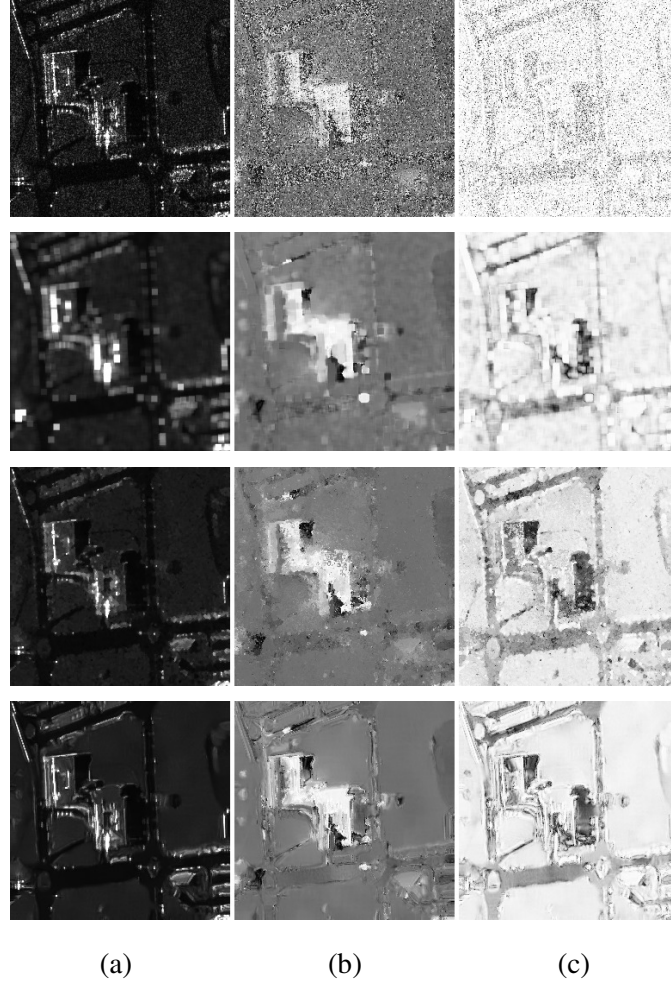
Figure 7.    (a) Reflectivity, (b) phase difference and (c) coherence of the CNES in Toulouse (France) ©DGA ©ONERA, obtained from top to bottom by the SLC images (maximum likelihood estimator of [28]), the boxcar estimator, the IDAN estimator [37] and the NL-InSAR estimator.

other filters for all components in term of SNR.

## B. Results on True SLC SAR Data

This section presents an overview of results obtained on a pair of co-registered real single-look complex SAR images with the same InSAR estimators as above. These images have been acquired over the CNES in Toulouse (France) sensed by RAMSES and provided by the CNES. The pair of SAR images is assumed to follow the Goodman's model presented in section I. In this experiment, the algorithms are executed with the same parameters as described in Section IV-A.

Figure 7 presents the obtained estimates for the different denoising filters. The results obtained with

our NL-InSAR estimator seem to be well smoothed with a better edge and shape preservation than other filters. For instance, IDAN is unable to restore the edges of the building when these edges are not present in the amplitude images even though these edges are present in the phase difference image. This is also the case for the three trees on the left side of the image. Since NL-InSAR considers both the information of amplitude and phase, NL-InSAR restores the edges and the trees successfully. The speckle effect is strongly reduced and the spatial resolution seems to be well preserved: buildings, streets, and homogeneous areas are well restored in the three parameter images. Moreover, the bright scatterers (numerous in urban area) are well restored. Note that NL-InSAR preserves well the three bright lines on the left of the building whereas the boxcar filter blurs them and IDAN attenuates them. This attests the efficiency of the patch-based approach: the three lines acts as a ramp on which the similarity patch slides in order to combine all pixels parallel to the bright lines. One can notice that very thin and dark structures are attenuated by NL-InSAR, such as the thin streets. This drawback might be avoided by using a smaller search window size to reduce the bias. In [16], [17], [35], [38]–[40], the authors propose to use adaptive search window size. Such approaches could be possibly used in NL-InSAR to reduce this undesired effect.

## V. CONCLUSION

A new method was proposed for SAR interferogram estimation. This method is based on the non-local means filter [24] whose originality rests on the combination of pixel values which can be far apart. We apply the general iterative methodology proposed in [14] to select suitable pixels by evaluating a patch-based similarity considering noisy amplitudes, noisy phase differences and previous estimates. Finally, the reflectivity, the actual phase difference and the coherence are jointly estimated. The proposed estimator out-performs the boxcar estimator and the IDAN estimator [23] in terms of both noise reduction and edge preservation. The noise, present in the input images, is well smoothed in the homogeneous regions and the object contours are well restored (preservation of the resolution). Moreover we can consider from our experiments that the reflectivity, the actual phase difference and the coherence are well recovered, without introducing strong undesired artifacts, with a good restoration of bright scatterers. A drawback of this estimator is the attenuation of thin and dark details in the regularized images. In a future work, we will try to better preserve these structures, by using adaptive patch-size selection. The filter elaboration, based on the statistics of the processed images, has led to define a suitable patch-similarity criterion for InSAR images. This similarity criterion could be applied in the future to other applications such as pattern tracking and displacement estimation.

November 5, 2009

## Appendix A

### Similarity Likelihood

The similarity likelihood is given by the triple integral

$$\mathcal{I}_3 = \iiint p(A_1, A_1', \phi_1 | R, D, \beta) p(A_2, A_2', \phi_2 | R, D, \beta) dR dD d\beta.$$

Starting the integration calculus on the variable $\beta$, the following simple integral has to be solved:

$$\mathcal{I}_1 = \int \exp\left[\lambda\left(A_1 A_1' \cos(\phi_1 - \beta) + A_2 A_2' \cos(\phi_2 - \beta)\right)\right] d\beta$$

with $\lambda = \frac{2D}{R(1-D^2)}$. Integrating by substitution $\psi \leftarrow \beta + \phi_2$ and developing the cosine functions gives:

$$\mathcal{I}_1 = \int \exp\left[\lambda\left(A_2 A_2' + A_1 A_1' \cos(\Delta\phi)\right)\cos(\psi) + \right.$$
$$\left. \lambda\left(A_1 A_1' \sin(\Delta\phi)\right)\sin(\psi)\right] d\psi$$

with $\Delta\phi = \phi_1 - \phi_2$. Then, by using eq. 3.937.2 in [41]:

$$\mathcal{I}_1 = 2\pi J_0\left(j \frac{2D\sqrt{A_1^2 A_1'^2 + A_2^2 A_2'^2 + 2A_1 A_1' A_2 A_2' \cos\Delta\phi}}{R(1-D^2)}\right)$$

with $J_n$ the Bessel function of the first kind. Pursuing on the variable $R$ gives the following integral:

$$\mathcal{I}_2 = \int \frac{1}{R^4} \exp\left(-\frac{A_1^2 + A_1'^2 + A_2^2 + A_2'^2}{R(1-D^2)}\right) \mathcal{I}_1 dR.$$

Using the integration by substitution $x \leftarrow 1/R(1-D^2)$ gives:

$$\mathcal{I}_2 = 2\pi(1-D^2)^3 \int x^2 \exp\left(-x(A_1^2 + A_1'^2 + A_2^2 + A_2'^2)\right)$$
$$J_0\left(jx2D\sqrt{A_1^2 A_1'^2 + A_2^2 A_2'^2 + 2A_1 A_1' A_2 A_2' \cos\Delta\phi}\right) dx.$$

According to eq. 6.621.4 in [41]:

$$\mathcal{I}_2 = 2\pi(1-D^2)^3 \left(\frac{2\mathcal{A} + D^2\mathcal{B}}{\sqrt{\mathcal{A} - D^2\mathcal{B}}^5}\right)$$
$$\text{with} \quad \mathcal{A} = (A_1^2 + A_1'^2 + A_2^2 + A_2'^2)^2$$
$$\text{and} \quad \mathcal{B} = 4(A_1^2 A_1'^2 + A_2^2 A_2'^2 + 2A_1 A_1' A_2 A_2' \cos\Delta\phi).$$

Finally, the triple integral can be expressed by the following single integral on the variable $D$:

$$\mathcal{I}_3 = \frac{32}{\pi^3}\mathcal{C} \int \frac{(1-D^2)(2\mathcal{A} + D^2\mathcal{B})}{\sqrt{\mathcal{A} - D^2\mathcal{B}}^5} dD.$$
$$\text{with} \quad \mathcal{C} = A_1 A_1' A_2 A_2'$$

Developing the expression and using integration by substitution $x \leftarrow D^2$, the following holds:

$$
\begin{aligned}
\mathcal{I}_3 \;=\;& \frac{32}{\pi^3}\mathcal{C}\left[\frac{1}{\sqrt{\mathcal{A}}^3}\int \frac{x^{-1/2}}{\sqrt{1-x\mathcal{B}/\mathcal{A}}^5}dx+\right. \\
& \frac{\mathcal{B}-2\mathcal{A}}{2\sqrt{\mathcal{A}}^5}\int \frac{x^{1/2}}{\sqrt{1-x\mathcal{B}/\mathcal{A}}^5}dx- \\
& \left.\frac{\mathcal{B}}{2\sqrt{\mathcal{A}}^5}\int \frac{x^{3/2}}{\sqrt{1-x\mathcal{B}/\mathcal{A}}^5}dx\right].
\end{aligned}
$$

According to eq 3.194.1 in [41]:

$$
\begin{aligned}
\mathcal{I}_3 \;=\;& \frac{32}{\pi^3}\mathcal{C}\left[\frac{1}{\sqrt{\mathcal{A}}^3}\left(2\,_2F_1(\frac{5}{2},\frac{1}{2};\frac{3}{2};\frac{\mathcal{B}}{\mathcal{A}})\right)+\right. \\
& \frac{\mathcal{B}-2\mathcal{A}}{2\sqrt{\mathcal{A}}^5}\left(\frac{2}{3}\,_2F_1(\frac{5}{2},\frac{3}{2};\frac{5}{2};\frac{\mathcal{B}}{\mathcal{A}})\right)- \\
& \left.\frac{\mathcal{B}}{2\sqrt{\mathcal{A}}^5}\left(\frac{2}{5}\,_2F_1(\frac{5}{2},\frac{5}{2};\frac{7}{2};\frac{\mathcal{B}}{\mathcal{A}})\right)\right]
\end{aligned}
$$

with $_2F_1$ an hyper-geometric function. Finally, by developing the hyper-geometric function, the triple integral is equal to:

$$
\mathcal{I}_3 \;=\; \frac{32\mathcal{C}}{\pi^3\sqrt{\mathcal{B}}^3}\left(\frac{\mathcal{A}+\mathcal{B}}{\mathcal{A}}\sqrt{\frac{\mathcal{B}}{\mathcal{A}-\mathcal{B}}}-\arcsin\sqrt{\frac{\mathcal{B}}{\mathcal{A}}}\right).
$$

## APPENDIX B

### SIMILARITY ON THE ESTIMATES

The similarity on the estimate is defined from the Kullback Leibler divergence between two data distribution $p(A, A', \Delta\phi|R_1, D_1, \beta_1)$ and $p(A, A', \Delta\phi|R_2, D_2, \beta_2)$. It is equivalent to consider the Kullback Leibler divergence between $p(z|\Sigma_1)$ and $p(z|\Sigma_2)$ with $\Sigma_k$ as defined in (2) and $R_k = R'_k$, $k = 1..2$. The Kullback Leibler divergence between two zero-mean complex circular Gaussian distributions is given by:

$$
D_{KL}(\Sigma_1|\Sigma_2) = \frac{2}{\pi}\left[\log\left(\frac{\det\Sigma_1}{\det\Sigma_2}\right)+tr\left(\Sigma_1^{-1}\Sigma_2\right)-2\right].
$$

The symmetrical version of the Kullback Leibler divergence is then:

$$
\begin{aligned}
SD_{KL}(\Sigma_1|\Sigma_2) \;=\;& D_{KL}(\Sigma_1|\Sigma_2)+D_{KL}(\Sigma_2|\Sigma_1) \\
\;=\;& \frac{2}{\pi}\left[tr\left(\Sigma_1^{-1}\Sigma_2\right)+tr\left(\Sigma_2^{-1}\Sigma_1\right)-4\right].
\end{aligned}
$$

Note that with $R_k = R'_k$, $k = 1..2$:

$$
\begin{aligned}
tr(\Sigma_1^{-1}\Sigma_2) \;=\;& 2\left[\frac{R_2(1-D_1D_2e^{j(\beta_1-\beta_2)})}{R_1(1-D_1^2)}\right], \\
tr(\Sigma_2^{-1}\Sigma_1) \;=\;& 2\left[\frac{R_1(1-D_2D_1e^{j(\beta_2-\beta_1)})}{R_2(1-D_2^2)}\right].
\end{aligned}
$$

Then the symmetrical Kullback Leibler divergence is given by:

$$SD_{KL}(\Sigma_1, \Sigma_2) = \frac{4}{\pi} \left[ \frac{R_1}{R_2} \left( \frac{1 - D_1 D_2 \cos(\beta_1 - \beta_2)}{1 - D_2^2} \right) + \right.$$
$$\left. \frac{R_2}{R_1} \left( \frac{1 - D_1 D_2 \cos(\beta_1 - \beta_2)}{1 - D_1^2} \right) - 2 \right]$$

## REFERENCES

[1] N. Bechor and H. Zebker, "Measuring two-dimensional movements using a single InSAR pair," *Geophysical Research Letters*, vol. 33, p. 16, 2006.

[2] N. Goodman, "Statistical analysis based on a certain multivariate complex Gaussian distribution (an introduction)," *Annals of Mathematical Statistics*, pp. 152–177, 1963.

[3] J.-S. Lee, "Speckle analysis and smoothing of synthetic aperture radar images," *Computer Graphics and Image Processing*, vol. 17, no. 1, pp. 24–32, September 1981.

[4] D. Kuan, A. Sawchuk, T. Strand, and P. Chavel, "Adaptive noise smoothing filter for images with signal-dependent noise," *IEEE Transactions on Pattern Analysis and Machine Intelligence*, vol. 7, no. 2, pp. 165–177, 1985.

[5] Y. Wu and H. Maître, "Smoothing speckled synthetic aperture radar images by using maximum homgeneous region filters," *Optical Engineering*, vol. 31, p. 1785, 1992.

[6] A. Lopes, E. Nezry, R. Touzi, and H. Laur, "Maximum a posteriori speckle filtering and first order texture models in SAR images," in *Geoscience and Remote Sensing Symposium, 1990. IGARSS'90.*, 1990, pp. 2409–2412.

[7] V. Frost, J. Stiles, K. Shanmugan, and J. Holtzman, "A model for radar images and its application to adaptive digital filtering of multiplicative noise," *IEEE Transactions on Pattern Analysis and Machine Intelligence*, vol. 4, pp. 157–166, 1982.

[8] R. Touzi, "A review of speckle filtering in the context of estimation theory," *IEEE Transactions on Geoscience and Remote Sensing*, vol. 40, no. 11, pp. 2392–2404, 2002.

[9] F. Argenti and L. Alparone, "Speckle removal from SAR images in the undecimated wavelet domain," *IEEE Transactions on Geoscience and Remote Sensing*, vol. 40, no. 11, pp. 2363–2374, 2002.

[10] T. Bianchi, F. Argenti, and L. Alparone, "Segmentation-Based MAP Despeckling of SAR Images in the Undecimated Wavelet Domain," *IEEE Transactions on Geoscience and Remote Sensing*, vol. 46, no. 9, pp. 2728–2742, 2008.

[11] M. Bhuiyan, M. Ahmad, and M. Swamy, "Spatially adaptive wavelet-based method using the Cauchy prior for denoising the SAR images," *IEEE Transactions on Circuits and Systems for Video Technology*, vol. 17, no. 4, pp. 500–507, 2007.

[12] H. Xie, L. Pierce, and F. Ulaby, "SAR speckle reduction using wavelet denoising and Markov random field modeling," *IEEE Transactions on Geoscience and Remote Sensing*, vol. 40, no. 10, pp. 2196–2212, 2002.

[13] A. Achim, P. Tsakalides, and A. Bezerianos, "SAR image denoising via Bayesian wavelet shrinkage based on heavy-tailed modeling," *IEEE Transactions on Geoscience and Remote Sensing*, vol. 41, no. 8, pp. 1773–1784, 2003.

[14] C. Deledalle, L. Denis, and F. Tupin, "Iterative Weighted Maximum Likelihood Denoising with Probabilistic Patch-Based Weights," *IEEE Transactions on Image Processing*, 2009.

[15] E. Trouvé, M. Caramma, and H. Maître, "Fringe detection in noisy complex interferograms," *Applied Optics*, vol. 35, no. 20, pp. 3799–3806, 1996.

[16] J. Bioucas-Dias, V. Katkovnik, J. Astola, and K. Egiazarian, "Absolute phase estimation: adaptive local denoising and global unwrapping," *Applied Optics*, vol. 47, no. 29, pp. 5358–5369, 2008.

[17] V. Katkovnik, J. Astola, and K. Egiazarian, "Phase local approximation (PhaseLa) technique for phase unwrap from noisy data," *IEEE Transactions on Image Processing*, vol. 17, no. 6, pp. 833–846, 2008.

[18] R. Touzi, A. Lopes, J. Bruniquel, and P. Vachon, "Coherence estimation for SAR imagery," *IEEE Transactions on Geoscience and Remote Sensing*, vol. 37, no. 1 Part 1, pp. 135–149, 1999.

[19] C. López Martínez, X. Fàbregas Cànovas, and E. Pottier, "Wavelet Transform-Based Interferometric SAR Coherence Estimator," *IEEE Signal processing letters*, vol. 12, no. 12, pp. 831–834, 2005.

[20] C. Gierull, D. Establ, and O. Ottawa, "Unbiased coherence estimator for SAR interferometry with application to moving target detection," *Electronics Letters*, vol. 37, no. 14, pp. 913–915, 2001.

[21] J. Lee, S. Cloude, K. Papathanassiou, M. Grunes, and I. Woodhouse, "Speckle filtering and coherence estimation of polarimetric SAR interferometry data for forest applications," *IEEE Transactions on Geoscience and Remote Sensing*, vol. 41, no. 10 Part 1, pp. 2254–2263, 2003.

[22] J. Lee, M. Grunes, and G. De Grandi, "Polarimetric SAR speckle filtering and its implication for classification," *IEEE Transactions on Geoscience and Remote Sensing*, vol. 37, no. 5 Part 2, pp. 2363–2373, 1999.

[23] G. Vasile, E. Trouvé, J. Lee, and V. Buzuloiu, "Intensity-Driven Adaptive-Neighborhood Technique for Polarimetric and Interferometric SAR Parameters Estimation," *IEEE Transactions on Geoscience and Remote Sensing*, vol. 44, no. 6, p. 1609, 2006.

[24] A. Buades, B. Coll, and J. Morel, "A Non-Local Algorithm for Image Denoising," *Computer Vision and Pattern Recognition, 2005. CVPR 2005. IEEE Computer Society Conference on*, vol. 2, 2005.

[25] H. Maitre, *Processing of Synthetic Aperture Radar Images*. Wiley-ISTE, 2008.

[26] J. Fan, M. Farmen, and I. Gijbels, "Local maximum likelihood estimation and inference," *Journal of the Royal Statistical Society. Series B, Statistical Methodology*, pp. 591–608, 1998.

[27] J. Polzehl and V. Spokoiny, "Propagation-separation approach for local likelihood estimation," *Probability Theory and Related Fields*, vol. 135, no. 3, pp. 335–362, 2006.

[28] M. Seymour and I. Cumming, "Maximum likelihood estimation for SAR interferometry," in *The 1994 International Geoscience and Remote Sensing Symposium.*, vol. 4, 1994, pp. 2272–2274.

[29] Y. Matsushita and S. Lin, "A Probabilistic Intensity Similarity Measure based on Noise Distributions," in *IEEE Conference on Computer Vision and Pattern Recognition, 2007. CVPR'07*, 2007, pp. 1–8.

[30] J. Lee, "Digital image smoothing and the sigma filter," *Computer Vision, Graphics, and Image Processing*, vol. 24, pp. 255–269, 1983.

[31] L. Yaroslavsky, *Digital Picture Processing*. Springer-Verlag New York, Inc. Secaucus, NJ, USA, 1985.

[32] C. Tomasi and R. Manduchi, "Bilateral filtering for gray and color images," in *Computer Vision, 1998. Sixth International Conference on*, 1998, pp. 839–846.

[33] A. Buades, B. Coll, and J. Morel, "A Review of Image Denoising Algorithms, with a New One," *Multiscale Modeling and Simulation*, vol. 4, no. 2, p. 490, 2005.

[34] P. Coupe, P. Yger, and C. Barillot, "Fast Non Local Means Denoising for 3D MR Images," *Lecture Notes In Computer Science*, vol. 4191, pp. 33–40, 2006.

[35] B. Goossens, H. Luong, A. Pižurica, and W. Philips, "An improved non-local denoising algorithm," in *Proc. Int. Workshop on Local and Non-Local Approximation in Image Processing (LNLA'2008), Lausanne, Switzerland*, 2008.

[36] J. Darbon, A. Cunha, T. Chan, S. Osher, and G. Jensen, "Fast nonlocal filtering applied to electron cryomicroscopy," *Biomedical Imaging: From Nano to Macro, 2008. ISBI 2008. 5th IEEE International Symposium on*, pp. 1331–1334, 2008.

[37] G. Vasile, E. Trouvé, J. Lee, and V. Buzuloiu, "Intensity-driven adaptive-neighborhood technique for polarimetric and interferometric SAR parameters estimation," *IEEE Transactions on Geoscience and Remote Sensing*, vol. 44, no. 6, pp. 1609–1621, 2006.

[38] G. Gilboa, N. Sochen, and Y. Zeevi, "Estimation of optimal PDE-based denoising in the SNR sense," *IEEE Transactions on Image Processing*, vol. 15, no. 8, pp. 2269–2280, 2006.

[39] C. Kervrann and J. Boulanger, "Local Adaptivity to Variable Smoothness for Exemplar-Based Image Regularization and Representation," *International Journal of Computer Vision*, vol. 79, no. 1, pp. 45–69, 2008.

[40] N. Azzabou, N. Paragios, and F. Guichard, "Uniform and textured regions separation in natural images towards MPM adaptive denoising," *Lecture Notes in Computer Science*, vol. 4485, p. 418, 2007.

[41] I. Gradshteyn, I. Ryzhik, and A. Jeffrey, *Table of integrals, series, and products*. Academic Press, 1980.